Materials Research Express

PAPER

Crystal and electronic structure studies on transparent conducting nitrides A_3N_2 (A = Mg, Zn and Sn) and Sn_3N_4

To cite this article: T Premkumar and R Vidya 2019 *Mater. Res. Express* **6** 055912

Materials Research Express

RECEIVED
22 November 2018

REVISED
9 January 2019

ACCEPTED FOR PUBLICATION
7 February 2019

PUBLISHED
20 February 2019

PAPER

Crystal and electronic structure studies on transparent conducting nitrides A_3N_2 (A = Mg, Zn and Sn) and Sn_3N_4

T Premkumar and R Vidya

Department of Medical Physics, Anna University, Sardar Patel Road, Chennai, 600025 India

E-mail: vidyar@annauniv.edu

Keywords: transparent conducting nitrides, electronic structure, effective mass

Abstract

Finding potential materials for solar cell applications is essential to reduce cost and enhance efficiency. We have employed Density Functional Theory (DFT) based calculations for novel nitrides of type A_3N_2 (A = Mg, Zn ans Sn) and Sn_3N_4 to find the ground state crystal and electronic structure. The structural parameters optimized by theoretical calculation are in good agreement with the experimental parameters. In order to obtain Sn_3N_2 and Sn_3N_4 experimentally, we are suggesting a new synthesis route from the calculated enthalpy of formation. The studied nitrides exhibit semiconductor behavior with direct band gaps. Band gap of 1.7 eV is obtained for Mg_3N_2 from GGA calculation. For Sn_3N_4 band gaps of 0.24 eV and 0.7 eV are obtained using GGA and LDA calculations, respectively, whereas GGA+U was used to obtain band gap in Zn_3N_2. The bonding behavior is analyzed in detail by using charge density and electron localization function plots. In addition, COHP (Crystal Orbital Hamiltonian Population) is utilized to retrieve bond strength values. Charge transfer from cation to anion decreases from Mg to Sn and correspondingly bond strength between the metal and Nitrogen atoms is also found to increase from Mg to Sn, which indicates increase in covalent nature of bonding from Mg to Sn. Zn_3N_2 is found to have the possibility for n-type as well as p-type doping because of the low effective mass of electrons and holes compared to other studied nitrides. Hence, Zn_3N_2 has suitable conductive properties to be used as a solar cell material.

1. Introduction

Solar energy is one of the most-viable renewable energy sources, conversion of solar energy into other forms of energy such as electrical and thermal takes place with the help of optoelectronic and solar thermal devices, respectively. The materials constituting the devices determine the efficiency and stability of such devices. Finding suitable optoelectronic materials for photovoltaic conversion with good efficiency is a big challenge for researchers.

Wide band gap and high electrical conductivity of transparent conducting (TC) materials make them attractive and useful for solar energy conversion. Hence these materials play important roles in solar cells as window as well as transparent electrical contacts. In addition, they are used in other optoelectronic devices like light emitting diodes, flat panel displays and optical sensors [1]. Thermal infra-red radiation is reflected by TC materials, which is useful for energy conserving windows and low emissivity windows [2].

Transparent Conducting Oxides (TCO) are in the frontier of the TC materials research. During the last few decades, the dominant TCOs have been Tin Oxide (SnO_2), Indium Oxide (In_2O_3), Indium doped Tin Oxide (ITO) and Zinc Oxide (ZnO), because of their high electrical conductivity and optical transparency. Recent development of optoelectronic devices needs a material with high chemical stability, high refractive index to reduce the light reflection loss at the interface and effective optical transparency for high efficiency solar cells [3]. As these requirements are difficult to achieve only using conventional TCO, the TC materials research is extended beyond TCOs. The nitride TCs are expected to have the ability to overcome these drawbacks of TCOs, as they are having wide and direct band gap, large bulk moduli, high carrier concentration, high electron

mobility and low production cost [3]. It is well known that, group III nitrides such as, GaN, AlN and InN have been studied extensively and are used in various optoelectronic applications.

Mg_3N_2 is a group-II metal nitride used as a catalyst in the preparation of silicon and boron nitride and also has interesting electronic properties. From neutron diffraction refinement Mg_3N_2 is shown to have cubic anti-bixibyte structure [4]. Experimental optical diffusion spectrum gives the band gap of 2.8 eV whereas theoretical study based on local spherical wave method using scalar relativistic Hamiltonian with LDA exchange correlation gives a direct band gap of 1.10 eV [5]. The high electrical conductivity of Mg_3N_2 is said to result from the Mg 3*s* and N 2*s* states present in the conduction band minimum [5]. Calculation with linear combination of atomic orbitals method shows Mg_3N_2 has an indirect band gap of 2.25 eV between Γ point and a point between Γ and N [6]. More investigation is needed to reveal band features, bonding nature and conductivity properties of Mg_3N_2.

Recently, the group II nitride compound Zn_3N_2 has been attracting more attention for optoelectronic applications. Zn_3N_2 has been reported with interesting properties such as, high carrier concentration [3, 7], low electron effective mass [$(0.08 \pm 0.03)m_o$] from non parabolic conduction band method [8] and $(0.29 \pm 0.05)m_o$ from FTIR reflective measurements [9], which leads to high electron mobility [3, 7, 8, 10]. The refractive index is found to be 2.0–2.8 from the reflectance measurements [9, 11], and 2.3–2.7 from optical measurements [12]. But the optical measurements of oxidized samples show a refractive index of 1.6–1.8 [12] and also the transmittance measurements of oxidized samples show a refractive index of 1.7–2.4 [13].

Various experimental studies report the direct band gap of Zn_3N_2 ranging from 1.01 eV to 3.44 eV. Temperature dependent Hall effect measurements [14] and reflectance measurements [15] of RF magnetron sputtered Zn_3N_2 thin films show a band gap of 1.01 eV, whereas optical measurements show the band gap value as 2.9–3.2 eV [3, 16]. By increasing the carrier concentration, band gap increases as a function of carrier concentration from 1.06 eV for the Zn_3N_2 thin films prepared by RF molecular beam epitaxy and chemical vapor deposition [9]. Absorption spectra of RF magnetron sputtered Zn_3N_2 thin films show the band gap of 1.23 eV [7], photo luminescence spectrum exhibits the band gap of 2.76 and 3.22 eV [17]. Optical measurements of DC magnetron sputtered Zn_3N_2 thin films show the band gap of 1.31–1.48 eV and 3.44 eV for oxidized and unoxidized samples, respectively [12]. Transmittance measurements of thin films prepared by RF plasma assisted pulsed laser deposition method shows 3.2 eV band gap [12].

Density Functional Theory (DFT) based calculations on Zn_3N_2 give different values of band gap depending on the different exchange correlation functional used. The band gap of Zn_3N_2 was calculated as 0.03, 0.62, 0.23 eV by functionals LDA, LDA+*U* and PBE+*U*, respectively [18]. The band gap value was improved by using exchange correlation functionals TB-mBJ, HSE06, PBE0, and G_oW_o to 0.95, 0.86, 1.48, and 1.15 eV, respectively [18]. It was found that oxygen contamination without intentional doping leads to high carrier concentration and large optical band gap [9] and oxygen doping makes Zn_3N_2 thin films become more conductive [3]. Another important property of Zn_3N_2 is, it may be converted to *p*-type ZnO under suitable thermal oxidation [3, 19–23], which is useful to make ZnO *p*-*n* homo junctions. The *p*-type conductivity in Zn_3N_2 is theoretically shown to be introduced by Cu substitution at N sites [24]. Hence more research efforts are needed to reveal conductivity from band features, hybridization and bonding nature of Zn_3N_2.

Recently one of the group-IV nitrides Sn_3N_4 has attracted attention due to its good semi-conducting and electro-chromic properties. Moreover nano-crystalline Sn_3N_4 is used as a negative electrode material for Li-ion and Na-ion batteries [25] which has high stability up to 370 °C in vacuum [26]. Hexagonal phase of Sn_3N_4 thin films prepared by RF magnetron sputtering shows *n*-type conductivity and absorption spectra gives an indirect optical band gap of 1.5 eV [27]. Optical measurement of reactive sputtered Sn_3N_4 thin films also gives the band gap of 1.5 eV [28]. Later the bulk Sn_3N_4 was prepared using chemical reaction of tin halides with potassium amide and refinement using x-ray and neutron diffraction revealed cubic spinel structure [29]. First principles total energy calculation with LDA exchange correlation functional also concurred with the cubic spinel structure but showed a direct band gap of 1.153 eV [30]. An orthogonalized linear combination of atomic orbital method with LDA calculation gave the band gap value of 1.29 eV [31]. DFT+GW with GGA exchange correlation provides the direct band gap of 1.54 eV, small electron effective mass of $0.18m_o$ and large hole effective mass of $12.9m_o$ [32], which leads to small hole diffusion length. Further research efforts are needed to develop Sn_3N_4 for semiconducting applications.

In this report, we present the results of DFT based calculations on A_3N_2 (A = Mg, Zn and Sn) and Sn_3N_4, on their structural stability and electronic structure properties such as, band structure, density of states (DOS), effective mass of charge carriers are analyzed in detail. Formation of bonds between constituent atoms is explored using charge density and electron localization function (ELF) plots. We have computed Crystal Orbital Hamiltonian Population (COHP) to explore bonding, anti-bonding states and bond strengths between any two constituent elements of the studied systems.

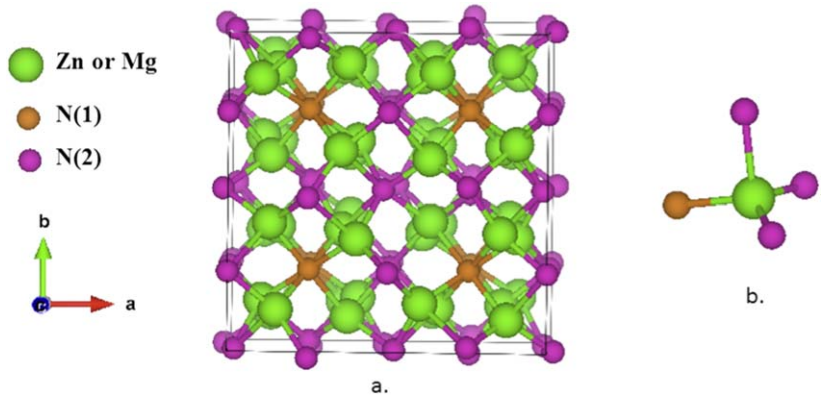

Figure 1. (a) Anti-bixibyte Crystal Structure. (b) Tetrahedral coordination of the metal atom.

2. Computational details

First principles calculations are used to explore the material properties based on projected augmented plane wave method [33] implemented in the Vienna *ab-initio* Simulation Package (VASP) [34]. All calculations are done using plane wave cutoff energy 400 eV for optimization and 550 eV for electronic structure calculations. The ions are completely relaxed with force and stress minimization with convergence criteria 10^{-6} eV per unit cell for total energy and $\leqslant 1$ meVÅ^{-1} for force minimization. The exchange correlation effects are treated under Local Density Approximation (LDA) [35] and Generalized Gradient Approximation (GGA) [36] with Perdew Burke Ehrenkof (PBE) functional. Strongly correlated materials are treated additionally with Hubbard U parameter based on simplified rotationally invariant approach to the LSDA+U [37] with various U values. The k-point grid of $8 \times 8 \times 8$ with Monkhrost-Pack [38] scheme was used throughout the calculations. Bond strengths between the constituent atoms are computed using COHP [39], which is implemented in the tight binding linear muffin-tin orbital (TBLMTO-47) package [40, 41]. The charge density and ELF obtained from VASP calculation are plotted using Vesta 3D visualization tool [42].

3. Results and discussion

3.1. Structural Properties

Experimental structural refinement of Mg_3N_2 and Zn_3N_2 was done by Partin *et al*, [4] The crystal structure of Mg_3N_2 and Zn_3N_2 is body centered cubic with space group $Ia\bar{3}$ (No: 206) known as anti-bixibyte structure. In this structure the metal atom occupies Wyckoff positions 48*e* and two different types of N [N(1) and N(2)] occupy the 8*b* and 24*d* Wyckoff positions, respectively. The conventional unit cell has 80 atoms, projected along *c*-axis (figure 1(a)). Every metal atom is surrounded by four nitrogen atoms forming tetrahedral co-ordination (figure 1(b)). Both types of N atoms are surrounded by six metal atoms, forming lightly distorted octahedral co-ordination. For the case of Sn_3N_2, experimental studies are hitherto not available. Hence we have predicted the structural parameters for Sn_3N_2 in the anti-bixibyte structure. We performed complete structural relaxation by starting with guessed structural parameters using ionic radii of Mg^{2+} and Zn^{2+}, as a scaling factor. We obtained the guessed structural parameters by extrapolating those of Mg_3N_2 and Zn_3N_2.

Sn_3N_4 crystallises in cubic spinel structure (figure 2(a)), with space group *Fd*-3*m* (No: 227) [29]. There are two types of metal atoms Sn(1) and Sn(2) occupying the 8*a* and 16*d* Wyckoff positions, and forms perfect tetrahedral (figure 2(b)) and octahedral(figure 2(c)) co-ordinations, respectively. The nitrogen atoms occupy the 32*e* Wyckoff positions and every nitrogen atom is surrounded by four metal atoms.

The experimental structural parameters (except for Sn_3N_2) are taken as initial parameters for complete structural optimization. The structural parameters obtained after force as well as stress minimization are tabulated in table 1. The theoretically optimized structural parameters are found to be in good agreement with experimental results and were used in our further calculations. Due to the over binding nature of LDA, calculated lattice parameters are underestimated compared to the experimental values by 1.5%, 2% and 0.5% for Mg_3N_2, Zn_3N_2 and Sn_3N_4, respectively. GGA overestimates the structural parameters compared to the experimental values by 0.4%, 0.8% and 1.2% for Mg_3N_2, Zn_3N_2 and Sn_3N_4, respectively. However, experimental lattice parameters are not yet available for Sn_3N_2. The optimized lattice parameters are overestimated than the assumed parameters. The effect of LDA and GGA on Sn_3N_2 will be known only, if experimental values become available.

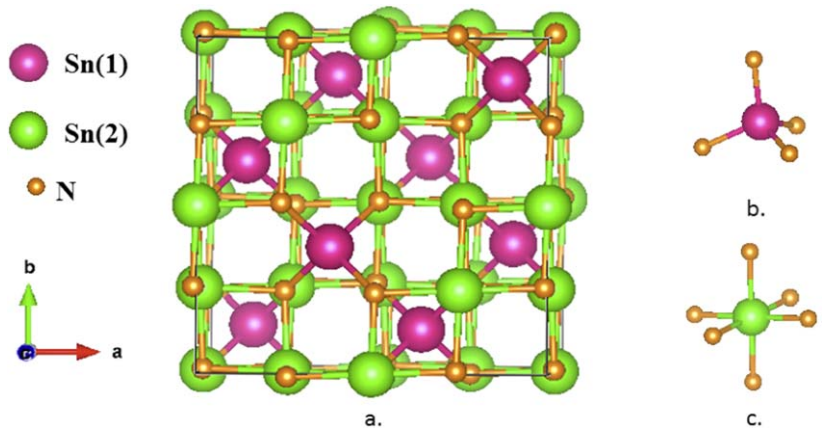

Figure 2. (a) Cubic spinel structure of Sn_3N_4. (b) Tetrahedral coordination of Sn(1). (c) Octahedral coordination of Sn(2).

Table 1. Calculated lattice parameter, formation energy and band gap of studied A_3N_2 (*A*: Mg, Zn and Sn) and Sn_3N_4 compounds.

Compounds	Lattice parameter(Å)			Formation energy (eV)	Band gap (eV)	
	LDA	GGA	Exp		Present	Experiment
Mg_3N_2	9.821	9.990	9.952 [4]	−4.059	1.7[b]	2.8 [5]
Zn_3N_2	9.593	9.847	9.769 [4]	−0.893	0[b], 0.13[c], 0.26[d], 0.4[e]	1.01–3.44 [3, 9, 12, 14–17]
Sn_3N_2	11.195	11.543	10.044[a]	−13.762	0	Not available
Sn_3N_4	8.992	9.139	9.037 [29]	−31.058	0.24[b], 0.7[f]	1.5 [28]

[a] Assumed lattice parameter.
[b] Based on GGA calculation.
[c] Based on GGA+U calculation with $U = 6$ eV.
[d] $U = 8$ eV.
[e] $U = 10$ eV.
[f] Based on LDA calculation

In order to find energetic stability of the compounds, we calculated formation energy which is given in table 1. Negative formation energy of both Mg_3N_2 and Zn_3N_2 confirms the formation of these compounds by passing the N_2 gas over the metal atoms. We considered the energetics of the following chemical reactions, for finding relative stability of Sn_3N_2 and Sn_3N_4.

$$3Sn + 2N_2 \longrightarrow Sn_3N_4$$
$$3Sn + N_2 \longrightarrow Sn_3N_2 \quad (1)$$

$$3Sn + 4NH_3 \longrightarrow Sn_3N_4 + 6H_2$$
$$3Sn + 2NH_3 \longrightarrow Sn_3N_2 + 3H_2 \quad (2)$$

The formation energy of Sn_3N_2 and Sn_3N_4 by equation (1) is found to be 2.39 eV and 1.21 eV respectively, On the other hand, by treating NH_3 with metallic Sn (equation 2) the formation energies are −13.762 and −31.058 for Sn_3N_2 and Sn_3N_4, respectively, indicating that chemical reaction given by equation (2) is more probable to occur. Sn_3N_4 is found to be more stable than Sn_3N_2, because $E_n[Sn_3N_4]$ (−43.801 eV) < $E_n[Sn_3N_{2+}N_2]$ (−26.503 eV). Usually Sn can have two oxidation states of Sn^{2+} and Sn^{4+}. Sn^{2+} oxidizes and converts into Sn^{4+} under ambient atmosphere, which leads to instability of Sn^{2+} compounds [43]. Lower formation energy of Sn_3N_4 from our energetic study also confirms that, Sn_3N_4 is more stable than Sn_3N_2, and other nitrides considered in this study.

3.2. Electronic structure properties

3.2.1. Band structure and DOS

In a solid, electrons are moving as waves in the electric field created by nuclei and nearest electron clouds. Wave functions corresponding to these moving electrons in different energy levels are plotted as a electronic band structure to explore the conductivity properties of solids. Integrating electronic band with respect to energy provides Density of States (DOS) within a given energy range, which elucidates contribution of an atom and its orbitals to the particular energy bands.

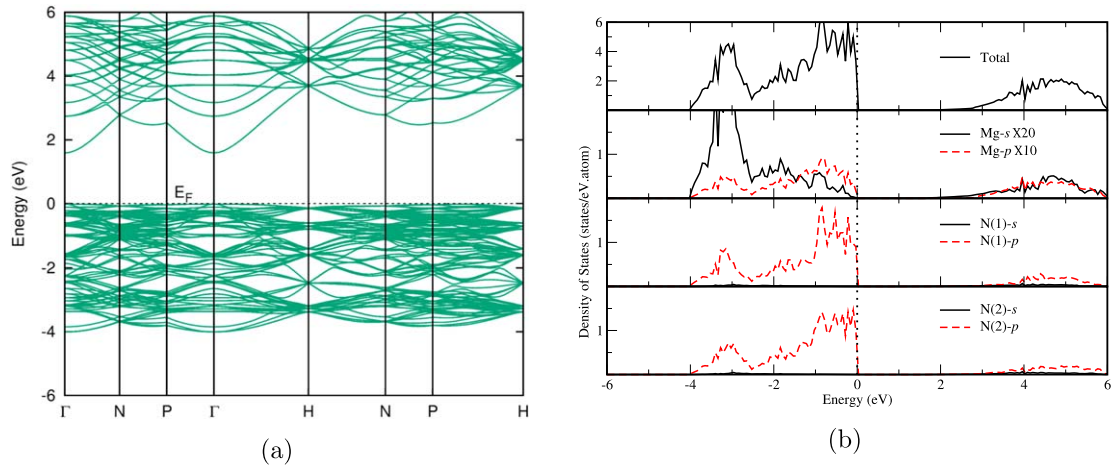

Figure 3. The calculated (a) Electronic band structure. (b) Total and partial DOS of Mg_3N_2 using GGA.

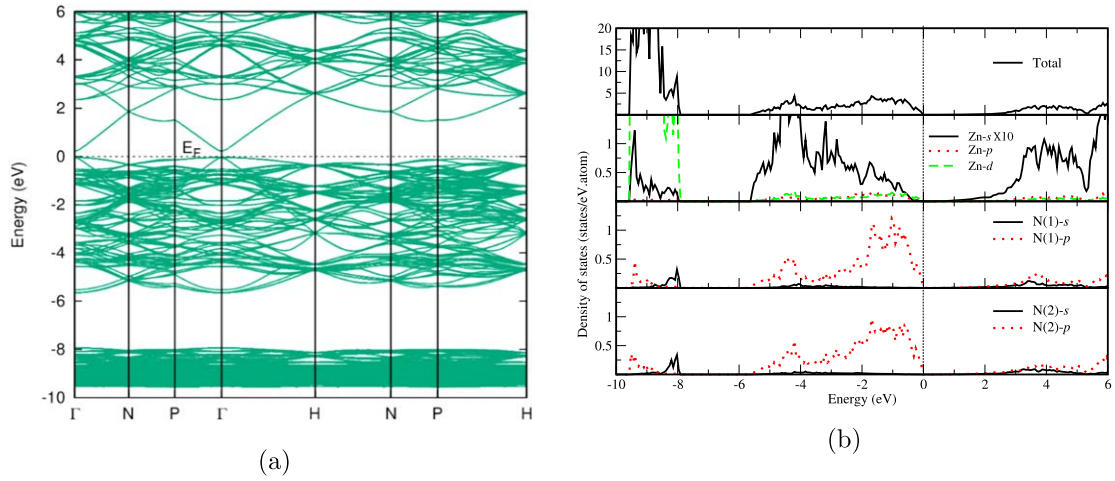

Figure 4. The calculated (a) Electronic band structure. (b) Total and partial DOS of Zn_3N_2 using GGA+U ($U = 8$ eV).

Electronic band structure (figure 3(a)) and total and partial DOS (figure 3(b)) for Mg_3N_2 are calculated using GGA exchange correlation functional. The valence band maximum (VBM) and conduction band minimum (CBM) occur at Γ point which implies a direct band gap with gap energy of 1.7 eV, whereas experimentally measured value is 2.8 eV [5]. It is well known that DFT usually underestimates the band gap. However, our result is in better agreement with experiment, compared to a study based on local spherical wave method with LDA, which gives the band gap of 1.10 eV [5]. Another theoretical study with linear combination of atomic orbitals showed an indirect band gap value of 2.25 eV [6]. DOS plot shows that the upper valence band of Mg_3N_2 extends from −4 eV to E_F and contains mostly N p states and small trace amount of Mg s and p states becomes visible only after multiplying by 10 and 20 times, respectively. This implies that Mg has donated its outer electrons to N, forming significant ionic bonding between Mg and N. The sharp peak near the E_F arises due to the presence of N p_y orbital states resulting in flat band at VBM. These localized energy states at VBM can increase the resistivity of p-type carriers in the material. Conduction band minimum is well dispersed due to the contribution of Mg 3s states, in agreement with previous theoretical work [5]. This dispersed nature of energy states provides high mobility to negative charge carriers, which is useful for photovoltaic applications.

Electronic band structure, total and partial DOS for Zn_3N_2 are shown in figures 4(a) and (b). Owing to strong correlation effects arising from Zn 3d orbital states, GGA was unable to show band gap in the calculated band structure. A similar DFT study using GGA was also unable to show band gap [24]. Hence we have performed additional calculations by including Hubbard U parameter into the exchange correlation functional. A small energy gap is opening up with values of 0.13, 0.26 and 0.4 for U values of 6, 8 and 10 eV, respectively. Our GGA+U calculation results are in compliance with already published theoretical results [18], but the band gap is

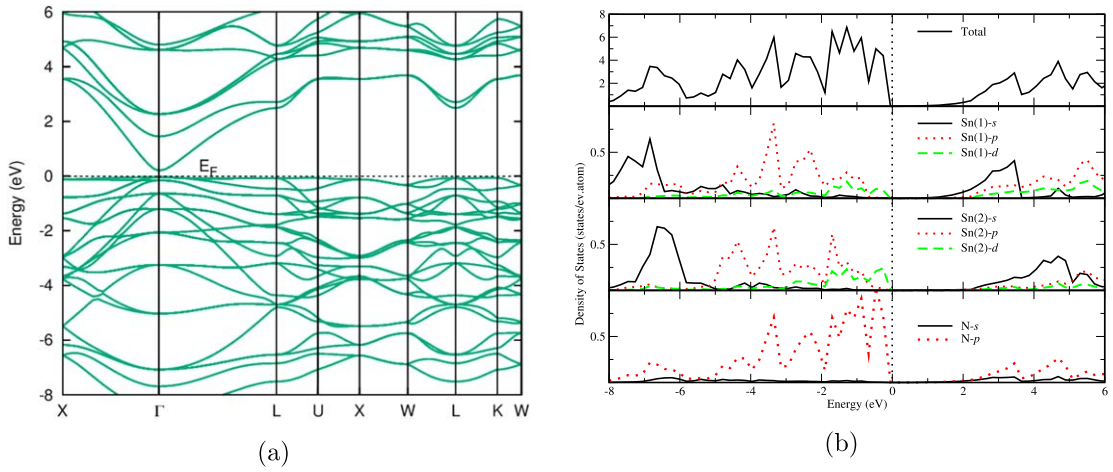

Figure 5. The calculated (a) Electronic band structure (b) Total and partial DOS of Sn_3N_4 using GGA.

still underestimated compared to the experimental values [3, 7, 9, 12, 14–16]. It is observed that the width of Zn 3*d* bands calculated using GGA+*U* is slightly narrower than that obtained using GGA.

The DOS calculated using GGA shows that the valence band is continuously distributed from −7.6 eV to E_F. High peaks are seen from −7.5 to −5.5 eV, due to the Zn 3*d* orbitals. By addition of Hubbard *U* with GGA, these continuously distributed DOS splits into two regions one from −9.6 to −7.9 eV and another one from −5.5 eV to E_F (figure 4(b)). Now the high peaks are seen from −9.6 to −7.9 eV due to the addition of Hubbard *U* with GGA. Due to the shift in these localized Zn 3*d* orbital states the whole valence band is pushed down from E_F and opens a gap between VBM and CBM. As in the zinc monochalcogenides [44], height of the Zn 3*d* orbital states calculated within GGA+*U* is more than the value calculated within GGA indicating that Zn 3*d* orbital states become more localized while applying onsite coulomb interaction with GGA. Calculated band gap with GGA+*U* has better agreement with experimental results than that from GGA indicating that strong correlation effects of Zn 3*d* electrons are important.

Orbital projected DOS calculated using GGA shows that the high peaks occurring in the region of −6.4 eV and −6 eV is due to Zn $3d_{x^2-y^2}$ and $3d_{z^2}$, respectively. There are significant amount of N 2*p* states also present in this energy range. Particularly there is a possibility for Zn $3d_{z^2}$ and N $2p_z$ orbitals to hybridize and produce significant covalent bond between these atoms. However, by including Hubbard *U* Zn 3*d* orbital states are shifted to lower energy range as described above. Consequently Zn $3d_{yz}$ and $3d_{zx}$ orbital states become more localized at −9 eV and −9.5 eV, respectively. Some of the N 2*p* states also shifted to lower energy levels due to the effect of Hubbard U with GGA. Small peak arising from N $2p_z$ states at −9.5 eV indicates its possibility to hybridize with Zn $3d_{zx}$ orbitals. In Zn_3N_2 also GGA+*U* shows less interaction between the orbitals compared to the results calculated using GGA, which indicates that originally the Zn_3N_2 might have more ionic type of bonding with non negligible covalent character. Because of N 2*p* orbital states VBM is less dispersed compared to CBM which is formed mostly due to Zn 4*s* orbital states. This dispersed band at CBM can lead to increase in the mobility of negative charge carriers. Hence with appropriate doping Zn_3N_2 can become *n*-type semiconducting material useful for photovoltaic applications.

Calculated electronic band structure for Sn_3N_2 elucidates its metallic behavior. Hence this material is not considered for further discussions. Electronic band structure (figure 5(a)) and total and partial DOS (figure 5(b)) for Sn_3N_4 are calculated and plotted. Direct band gap of 0.7 eV and 0.24 eV is observed at the Γ point from LDA and GGA calculations, respectively. Our calculated band gap is highly underestimated while comparing to the experimental band gap of 1.5 eV obtained using optical spectra [28] and theoretically calculated band gaps of 1.15 eV [30], 1.29 eV [31] and 1.54 eV [32]. Total DOS shows that the valence band extends from −9 eV to E_F. As the core levels are not involved in bonding, we have plotted DOS from −8 eV to E_F. Partial DOS shows that lower part of the valence band from −8 eV to −6 eV is mostly constituted by Sn *s* orbital states. Above −6 eV to E_F energy states are mostly due to the *p* orbital of Sn and N and there is a small contribution from Sn *d* orbital states. The peak occurring at −3.5 eV is due to Sn(1) p_x, p_z, Sn(2) p_y and N p_y orbitals. The energetic and spatial degeneracy between N p_y and Sn(2) p_y states indicates that these two orbitals have the possibility to hybridize with each other. The small peak due to N p_z and Sn(1) p_z orbitals is observed at −2.5 eV, which also indicates the hybridization between these two orbitals. Above −2 eV to E_F most of the states are due to N *p* orbital states, particularly due to N p_x orbital states and there is a small amount of Sn(2) *d* orbital states also present in this energy range. In [45], vanadium oxides are studied which have both tetrahedral and octahedral coordination.

Table 2. Calculated effective mass of the nitrides using finite difference method.

Compounds	Electron (m_o)	Heavy hole (m_o)	Light hole (m_o)
Mg_3N_2	0.195(Γ-H)	29.428(Γ-H)	7.647(Γ-H)
Zn_3N_2	0.076(Γ-H)	1.196(Γ-H)	1.133(Γ-H)
Sn_3N_4	0.093(Γ-K)	18.610(Γ-K)	0.605(Γ-K)

Owing to the distortion in the octahedra the t_2g and e_g orbitals are shown to be mixed. Similarly Sn_3N_4 has both tetrahedral as well as octahedral coordination without any distortion. But here no splitting of 4*d* orbitals is seen because, all the 4*d* orbitals are completely filled, leading to spherical distribution. Due to the presence of N *p* orbitals, the VBM is less dispersed compared to the CBM which is constituted by Sn *s* orbitals. This dispersed band at CBM provides more conductivity to negative charge carriers, compared to the holes in VBM. Hence, Sn_3N_4 might become good *n*-type semiconductor material by substitution of a suitable impurity.

3.2.2. Effective mass calculation

Effective mass is one of the best descriptors of mobility and conductivity of charge carriers. Charge carriers moving inside the solids (through the electric field created by ions) will have a momentum described by $\vec{p} = m_0\vec{v}$ where m_0 is rest mass of an electron and $\vec{v}$ is its velocity. Effective mass determines the effects of an external force due to crystal lattice on the momentum of moving charge carriers, which can be calculated using $\frac{1}{m^*} = \frac{1}{\hbar^2}\frac{d^2E}{dk^2}$ from the E(k) relation. Several methods are employed in the calculation of effective mass, such as parabolic curve fitting method, finite difference method, etc. We calculated effective masses for the studied nitrides along specific direction using the finite difference method and the values are given in table 2. As the CBM of above studied nitrides are well dispersed, the calculated electron effective masses are small. The calculated effective mass of Zn_3N_2 is in good agreement with the experimental effective mass of $(0.08 \pm 0.03)m_o$ obtained from non parabolic conduction band method [8]. However FTIR reflective measurements gave an effective mass of $(0.29 \pm 0.05)m_o$ [9]. Zn_3N_2 should exhibit high *n*-type conductivity, because of less electron effective mass while comparing with Mg_3N_2 and Sn_3N_4. Mg_3N_2 and Sn_3N_4 also have low electron effective mass but their heavy hole effective mass is very large, $29.43m_0$ and $18.61m_0$ for Mg_3N_2 and Sn_3N_4, respectively. This heavy hole effective mass leads to short hole diffusion length, which in turn decreases the efficiency of solar cells. Heavy hole effective mass of Zn_3N_2 is almost equal to rest mass of the electron but, less compared to the heavy hole effective masses of Mg_3N_2 and Sn_3N_4. Light hole effective mass of Zn_3N_2 is slightly lesser than its heavy hole effective mass corresponding to disperse nature of bands occurring at the Γ point. As both the heavy hole and light hole have low effective masses, Zn_3N_2 can be a potential candidate for *p*-type doping. Hence, Zn_3N_2 could be a favorable material for solar cell applications.

3.3. Electron distribution and bonding analysis

Bonding nature between any two constituent atoms in a solid can be understood by plotting the charge density around these atoms in real space lattice. Electron localization function plots provides the paired electron distribution for multi electron systems in a real space. Combining charge density and ELF analysis throws more light on the bonding nature. Plotted charge density and ELF for Mg_3N_2 (figures 6(a) and (d)) show that presence of electronic density around N rather than Mg, implying that Mg donates its outer electrons to N and forms significant ionic bond with N. This is consistent with electronegativity difference value of 1.73 between Mg and N.

Calculated charge density and ELF for Zn_3N_2 (figures 6(b) and (e)) shows that non negligible electron density is present between Zn and N. More electron density is seen around N from ELF indicates that Zn donates most of its electrons to N and forms mostly ionic bond with non negligible covalency between Zn and N, consistent with the DOS analysis. Electronegativity difference between Zn and N (1.39) is less than the eletronegativity difference between Mg and N (1.73) implies, decrease in ionic character of the bonding between Zn and N.

Charge density and ELF plots for Sn_3N_4 are shown in figures 6(c) and (f). Charge density between Sn and N indicates the sharing of electrons between Sn and N. As the charge density distribution is almost homogeneous the electron density description using LDA is better than that by GGA. This may be one of the reasons why the band gap obtained by LDA is more than that by GGA (table 1), Similar to the band gap values in $ASnO_3$ (A: Ba, Ca, Cd and Sr) [46]. There are two types of Sn as described in section 3.1. ELF with isosurface value of 0.65 shows more electron clouds between Sn(1) and N compared to that between Sn(2) and N. This implies that Sn(1) and N form bonds with more covalent character. On the other hand, ELF around Sn(2) is less than that around Sn(1) as well as around N. This indicates that Sn(2) could have donated its electrons to N, in addition to sharing some

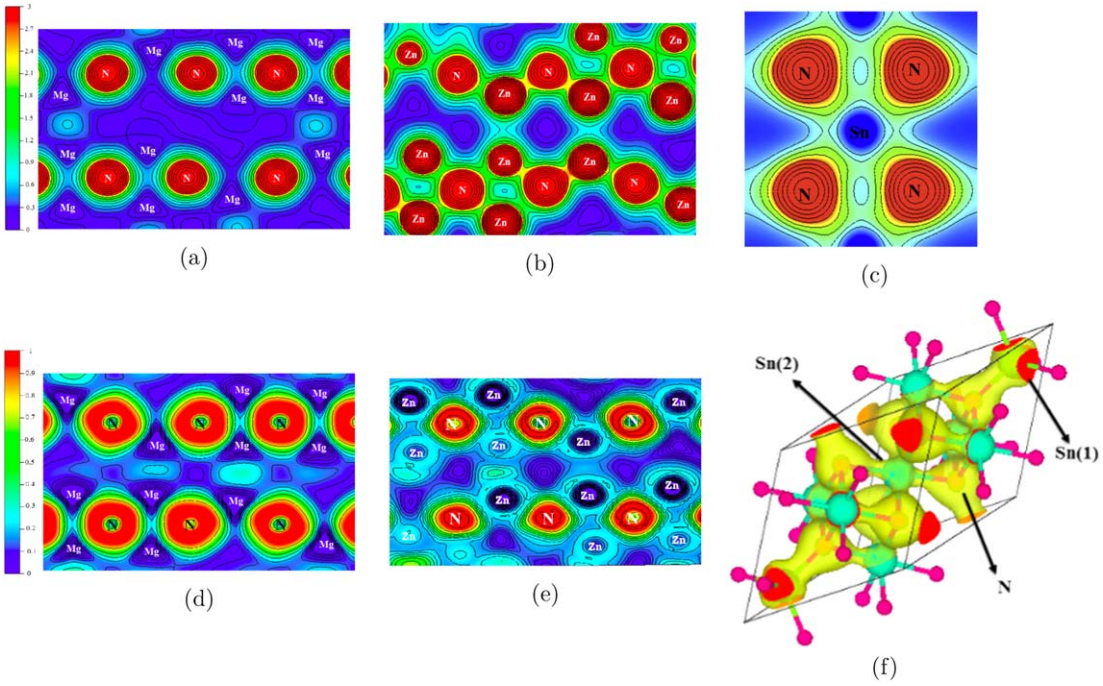

Figure 6. Charge density (a)–(c) and ELF (d)–(f) for the compounds Mg_3N_2, Zn_3N_2 and Sn_3N_4, respectively.

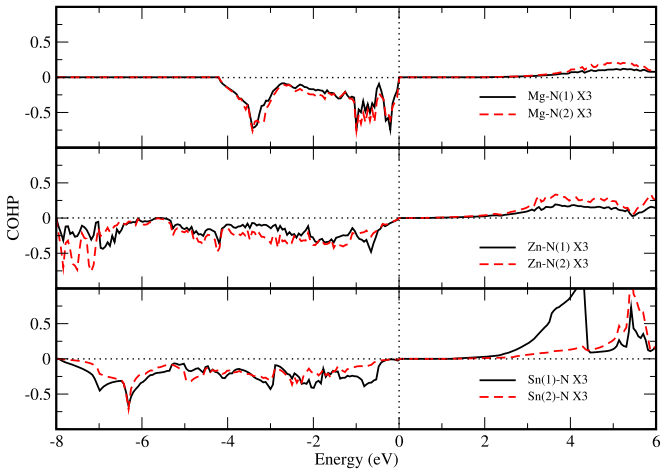

Figure 7. Crystal Orbital Hamiltonian Population plots.

electrons with N neighbours. Thus Sn(2) and N could form mixed iono-covalent bond. Electronegativity difference between Sn and N (1.08) also signals the formation of covalent bond between Sn and N. Our bonding analysis shows increasing covalent nature of bonding from Mg to Sn.

3.4. Crystal orbital Hamiltonian population (COHP)

COHP derives the orbital pair interaction from the band structure energy or the bond weighted density of states between a pair of adjacent atoms. COHP provides the bonding and anti-bonding states to the band structure energy [39]. Negative value of COHP corresponds to bonding states and positive value of COHP corresponds to anti-bonding states. Usually the number of electrons in a particular energy range is derived by integrating the DOS in that energy. Similarly the specific bond strength between two interacting atoms is explored from integrated COHP (ICOHP) values. We have plotted COHP (figure 7) between Mg-N(1), Mg-N(2), Zn–N(1), Zn–N(2), Sn(1)–N and Sn(2)–N from −8 eV to 6 eV energy range. Bonding states are distributed from −4 eV to E_F for Mg_3N_2 and from −8 eV to E_F for both Zn_3N_2 and Sn_3N_4. ICOHP values up to E_F provide the bond strength between the interacting atoms. Evaluated bond strengths along with corresponding bond lengths are tabulated in table 3. Less number of bonding states are seen between Mg-N(1) and Mg-N(2) than those between

Table 3. Calculated bond lengths and their corresponding bond strengths.

Compounds	Bond length (Å)	Bond strength (eV)
Mg-N(1)	2.145	−1.464
Mg-N(2)	2.086	−1.740
(3 types)	2.160	−1.443
	2.179	−1.338
Zn–N(1)	2.132	−1.764
Zn–N(2)	1.997	−2.562
(3 types)	2.069	−2.172
	2.262	−1.122
Sn(1)–N	4⊗2.105	−2.575
Sn(2)–N	6⊗2.177	−2.041

Zn–N and Sn–N bonding states, implying weaker bonds between Mg and N. Small bond strength arises because, electrons are transferred from Mg to N rather than sharing of electrons as indicated by our charge density and ELF analysis. In Zn_3N_2, Zn–N(2) has more bonding states than Zn–N(1) implying stronger bond formation between Zn and N(2). Similarly, in Sn_3N_4, Sn(1)–N has more bonding states than Sn(2)–N also confirms the stronger bond strength between Sn(1) and N. It can be seen that shorter bonds have more strength. In Mg_3N_2 and Zn_3N_2 the bonding is mostly ionic in nature, there are no significant σ and π bonding formation but, in the case of Sn_3N_4 there is a possibility to form σ and π bonds. In the bonding states the energetically as well as spatially degenerate p_y orbitals of Sn and N have the possibility to form π bond in the energy range from −3.5 to −3 eV and p_z orbitals of Sn and N also have the possibility to form σ bond in the energy range from −2.5 to −2 eV. In the anti-bonding states there is a possibility to form σ bond between *s* orbitals of Sn and N. Among all the bonds considered, bond lengths of Zn–N(2) and Sn(1)–N are shorter. Hence they form stronger bonds, which is consistent with ELF analysis. Zn_3N_2 and Sn_3N_4 are more stable than Mg_3N_2. Increase in bond strength from Mg to Sn confirms the domination of covalent nature of bonding. Sn_3N_4 is more covalent than Zn_3N_2 whose covalent bond is stronger than Mg_3N_2.

4. Conclusion

We have analyzed structural, electrical and bonding properties of group II nitrides of type A_3N_2 (A = Mg, Zn ans Sn) and group IV nitride (Sn_3N_4) using first principles calculations. Optimized structural parameters are consistent with the available experimental results. We suggested a new route to synthesize Sn_3N_4 and Sn_3N_2 from our energetic study and metallic nature of Sn_3N_2 also explained. Semiconductor behavior of nitrides was explored with direct band gaps. Experimentally Mg_3N_2 and Zn_3N_2 are shown as wide band gap semiconductors, but our calculations provide underestimated band gap values. Zn 3d electrons strongly affect the valence band leading to underestimation of the band gap. However, calculation with GGA+U improves the band gap value in agreement with previous theoretical work. The importance of adding a strong correlation parameter is realized through this study. Sn_3N_4 has optimum band gap to convert the visible light to electrical energy, but the high hole effective mass may decrease its efficiency. Zn_3N_2 has the lowest electron effective mass and small hole effective mass among the three nitrides. So Zn_3N_2 can be doped as *p*-type as well as *n*-type conducting material. Increase in covalent nature of bonding from Mg to Sn is observed. High bond strength of Zn_3N_2 and Sn_3N_4 proves good stability of these materials. Abundance of Zn and N is very advantageous to develop Zn_3N_2 as a cost effective solar cell material in future.

Acknowledgments

Authors are grateful to DST-SERB, India for providing financial support through the project SB/FTP/PS-009/2014 under the DST-Young Scientist Scheme, and Anna University for computer facilities (Procs. No 4137/PD4/2015).

ORCID iDs

T Premkumar https://orcid.org/0000-0002-0130-4984
R Vidya https://orcid.org/0000-0002-7798-1797

References

[1] Ginley D S and Bright C 2000 *MRS Bull.* **25** 15
[2] Gordon R G 2000 *MRS Bull.* **25** 52
[3] Yamada N, Watarai K, Yamaguchi T, Sato A and Ninomiya Y 2014 *Jpn. J. Appl. Phys.* **53** 05FX01
[4] Partin D E, Williams D J and O'Keeffe M 1997 *J. Solid State Chem.* **132** 56–9
[5] Fang C M, de Groot R A, Bruls R J, Hintzen H T and de With G 1999 *J. Phys: Condens. Matter.* **11** 4833
[6] Moreno Armenta M G, Reyes-Serrato A and Avalos Borja M 2000 *Phys. Rev.* B **62** 4890–8
[7] Futsuhara M, Yoshioka K and Takai O 1998 *Thin Solid Films* **322** 274–81
[8] Cao X, Yamaguchi Y, Ninomiya Y and Yamada N 2016 *J. Appl. Phys.* **119** 025104
[9] Suda T and Kakishita K 2006 *J. Appl. Phys.* **99** 076101
[10] Cao X, Sato A, Ninomiya Y and Yamada N 2015 *J. Phys. Chem.* C **119** 5327–33
[11] Garcia C, Piqueras J, Dez M J H, Nunez M C and Piqueras J 2011 *Appl. Phys. Lett.* **99** 232112
[12] Trapalis A, Heffernan J, Farrer I, Sharman J and Kean A 2016 *J. Appl. Phys.* **120** 205102
[13] Ayouchi R, Casteleiro C, Santos L and Schwarz R 2010 *Phys. Status Solidi* C **7** 2294–7
[14] Xing G Z, Wang D D, Yao B, Qune L F N A, Yang T, He Q, Yang J H and Yang L L 2010 *J. Appl. Phys.* **108** 083710
[15] Toyoura K, Tsujimura H, Goto T, Hachiya K, Hagiwara R and Ito Y 2005 *Thin Solid Films* **492** 88–92
[16] Kuriyama K, Takahashi Y and Sunohara F 1993 *Phys. Rev.* B **48** 2781–2
[17] Zong F, Ma H, Ma J, Du W, Zhang X, Xiao H, Ji F and Xue C 2005 *Appl. Phys. Lett.* **87** 233104
[18] Yoo S H, Walsh A, Scanlon D O and Soon A 2014 *RSC Adv.* **4** 3306–11
[19] Wang D, Liu Y, Mu R, Zhang J, Lu Y M, Shen D Z and Fan X W 2004 *J. Phys: Condens. Matter* **16** 4635–42
[20] Bar M *et al* 2009 *Appl. Phys. Lett.* **94** 012110
[21] Erdogan N, Kara K, Ozdamar H, Esen R and Kavak H 2013 *Appl. Surf. Sci.* **271** 70–6
[22] Long R, Dai Y, Yu L, Guo M and Haung B 2007 *J. Phys. Chem.* B **111** 3379–83
[23] Kambilafka V, Voulgaropoulou P, Dounis S, Iliopoulos E, Androulidki M, Saly V, Ruzinsky M and Aperathis E 2007 *Superlattice. Microst.* **42** 55–61
[24] Jiang N, Roehl J L, Khare S V, Georgiev D G and Jayatissa A H 2014 *Thin Solid Films* **564** 331–8
[25] Li X, Hector A L, Owen J R and Shah S I U 2016 *J. Mater. Chem.* A **4** 5081–7
[26] Lima R S, Dionisio P H, Moro J T and Schreiner W H 1994 *Hyperfine Interact.* **83** 315–9
[27] Inoue Y, Nomiya M and Takai O 1998 *Vacuum* **51** 673–6
[28] Maruyama T and Morishita T 1995 *J. Appl. Phys.* **77** 6641–5
[29] Scotti N, Kockelmann W, Senker J, Trael S and Jacobs H 1999 *Z. Anorg. Allg. Chem.* **625** 1435–9
[30] Huang M and Feng Y P 2004 *J. Appl. Phys.* **96** 4015–7
[31] Ching W Y, Mo S D, Ouyang L, Rulis P, Tanaka I and Yoshiya M 2002 *J. Am. Ceram. Soc.* **85** 75–80
[32] Caskey C M, Seabold J A, Stevanovic V, Ma M, Smith W A, Ginley D S, Neale N R, Richards R M, Lany S and Zakutayev A 2015 *J. Mater. Chem.* C **3** 1389–96
[33] Blöchl P E 1994 *Phys. Rev.* B **50** 17953–79
[34] Kresse G and Furthmuller J 1996 *Comput. Mater. Sci.* **6** 15–50
[35] Perdew J P and Zunger A 1981 *Phys. Rev.* B **23** 5048–79
[36] Perdew J P, Burke S and Ernzarhof M 1996 *Phys. Rev. Lett.* **77** 3865–8
[37] Dudarev S L, Botton G A, Savrasov S Y, Humphreys C J and Sutton A P 1998 *Phys. Rev.* B **57** 1505–9
[38] Monkhorst H and Pack J 1976 *Phys. Rev.* B **13** 5188–92
[39] Dronskowski R and Bloechl P E 1993 *J. Phys. Chem.* **97** 8617–24
[40] Andersen O K 1975 *Phys. Rev.* B **12** 3060–83
[41] Andersen O K and Jepsen O 1984 *Phys. Rev. Lett.* **53** 2571–4
[42] Momma K and Izumi F 2011 *J. Appl. Cryst.* **44** 1272–6
[43] Leijtens T, Prasanna R, Gold-Parker A, Toney M F and McGehee M D 2017 *ACS Energy Lett.* **2** 2159–65
[44] Karazhanov S Z, Ravindran P, Kjekshus A, Fjellvag H, Grossner U and Svensson B G 2006 *J. Appl. Phys.* **100** 043709
[45] Szymanski N, Liu Z, Alderson T, Podraza N, Sarin P and Khare S 2018 *Comput. Mater. Sci.* **146** 310–8
[46] Moreira E, Henriques J M, Azevedo D L, Caetano E W S, Freire V N, Fulco U L and Albuquerque E L 2012 *J. Appl. Phys.* **112** 043703